Journal Name

ARTICLE

Nano-assemblies of cationic mPEG brush block copolymers with gadolinium polyoxotungstate $[Gd(W_5O_{18})_2]^{9-}$ form stable, high relaxivity MRI contrast agents

Received 00th January 20xx,
Accepted 00th January 20xx

DOI: 10.1039/x0xx00000x

www.rsc.org/

Joanne Ly,[a,b] Yuhuan Li, [a,b] Mai N. Vu,[a,b] Bradford A. Moffat[c], Kevin S. Jack[d], John F. Quinn,[a,b] Michael R. Whittaker*[a,b] and Thomas P. Davis*[a,b,e]

Polyoxometalates (POMs) incorporating paramagnetic ions, such as gadolinium, show promise as contrast agents for application in magnetic resonance imaging (MRI). Specifically, $[Gd(W_5O_{18})_2]^{9-}$ (denoted as GdWO) has been reported to have a higher relaxivity than commercially available contrast agents, but it's clinical utility has been limited by the intrinsic instability of POMs at physiological pH (7.4). In the current report we present a stability study on neat GdWO and nano-assemblies of block copolymers with GdWO in the pH range 5.0-7.4 to assess their suitability as MRI contrast agents. Neat GdWO only maintained structural stability between pH 5.4 and 6.4, and demonstrated poor MRI contrast at pH 7.4. To address this pH instability, GdWO was self-assembled with cationic mPEG brush block copolymers containing 20 or 40 units derived from the cationic monomer, 2-dimethylaminoethyl methacrylate (DMAEMA). Nano-assemblies with different charge ratios were synthesised and characterised according to their size, stability, contrasting properties and toxicity. The longitudinal relaxivity (r_1) of the nano-assemblies was found to be dependent on the charge ratio, but not on the length of the cationic polymer block. Further investigation of $PDMAEMA_{20}$ nano-assemblies demonstrated that they were stable over the pH range 5.0-7.4, exhibiting a higher r_1 than either neat GdWO (2.77 $s^{-1}mM^{-1}$) or clinical MRI contrast agent Gd-DTPA (4.1 $s^{-1}mM^{-1}$) at pH 7.4. Importantly, the nano-assembly with the lowest charge ratio (0.2), showed the highest r_1 (12.1 $s^{-1}mM^{-1}$) whilst, stabilising GdWO over the pH range studied, eliciting low toxicity with MDA-MB231 cells.

Introduction

Biomedical imaging is an important diagnostic tool that can provide basic physiological, anatomical and molecular information for the detection, diagnosis and monitoring of disease states. Current imaging techniques include magnetic resonance imaging (MRI), positron emission tomography (PET), single photon emission computed tomography (SPECT), computer X-ray tomography (CT), optical imaging and ultrasound.[1-3] Since its inception in the early 1970s,[4, 5] MRI has emerged as an invaluable imaging modality with widespread clinical application in neurological, musculoskeletal, cardiovascular and oncological imaging. From 1995 to 2015, the number of MRI scans in the USA alone increased from 1 in 29 people to 1 in 9 people.[6] The popularity of MRI is due to the technique's high spatial resolution, non-invasiveness, and the fact that patients are not exposed to ionising radiation during the collection of the images.[7, 8] To improve contrast, the conspicuity of some pathology and improve the specificity of the diagnosis, approximately 30% of MRI scans require the use of a contrast agent to improve the quality of images.[9]

Contrast agents improve the contrast between different tissues by providing enhanced proton spin-lattice (T_1) and spin-spin (T_2) relaxation pathways, and hence shortening the relaxation time. The effect of the contrast agent on the T_1 and T_2 relaxation pathway is described by the longitudinal relaxivity (r_1) and transverse relaxivity (r_2), with a high relaxivity value indicating a larger effect on the relaxation. The most clinically used contrast agents are chelated gadolinium ions (such as Gd-DTPA, Gd-DOTA, Gd-DO3A, etc.). Gadolinium ions are paramagnetic, and enhance contrast because of the strong dipole-dipole interactions between their lone electron and the water protons in their hydration sphere. To abrogate their associated toxicity, gadolinium ions are generally complexed with either a linear or cyclic chelating agent.[9, 10] Nevertheless, exposure to chelated gadolinium ions can still trigger cases of nephrogenic systemic fibrosis for MRI patients with compromised kidney function.[11]

To further improve contrast and decrease systemic toxicity, research groups have focused on incorporating chelated gadolinium ions into nanoparticles. These hybrid nanoparticles, including silica nanoparticles,[12, 13] gold nanoparticles,[14, 15]

[a] ARC Centre of Excellence in Convergent Bio-Nano Science & Technology, Monash Institute of Pharmaceutical Sciences, Monash University, 381 Royal Parade, Parkville, Victoria 3052, Australia.
[b] Drug Delivery, Disposition and Dynamics, Monash Institute of Pharmaceutical Science, Monash University, 381 Royal Parade, Parkville, VIC 3052, Australia.
[c] Melbourne Brain Centre Imaging Unit, Department of Anatomy and Neuroscience, The University of Melbourne, Parkville 3010 Victoria, Australia.
[d] Centre for Microscopy and Microanalysis, The University of Queensland, St Lucia, QLD 4072, Australia.
[e] Department of Chemistry, University of Warwick, Gibbet Hill, Coventry, ULCV4 7AL, United Kingdom

† Electronic Supplementary Information (ESI) available: XPS, TGA curve, UV-Vis spectra, GPC trace, DLS particle size and ζ-potential, TEM images and cytotoxicity. See DOI: 10.1039/x0xx00000x

zeolites,[16] titanium dioxide,[17] polymeric nanospheres,[18-20] and star polymers,[21, 22] show increased relaxivity and lower toxicity compared to commercially available products (such as Gadovist®). Recently, there has been an interest in gadolinium-based nanoparticles as MRI contrast agents. For instance, gadolinium oxide (Gd_2O_3) nanoparticles,[23, 24] gadolinium phosphate ($GdPO_4$) nanoparticles,[25] sodium gadolinium fluoride ($NaGdF_4$) nanoparticles,[26, 27] gadolinium metal-organic framework (MOF) nanoparticles,[28-31] and polyoxometalates containing gadoliniums ions (Gd-POMs) have each been reported to have higher relaxivities, the smaller the nanoparticles. Of particular interest to us have been Gd-POMs due to their promising properties for application as a contrast agent.

Polyoxometalates (POMs) are inorganic metal-oxygen clusters formed from metal oxide polyhedral units of early transition metals, such as tungsten, molybdenum, vanadium, chromium, niobium or tantalum. Since their discovery in 1829 by Berzelius,[32] a range of POMs with different structure and chemical composition have been identified and investigated for applications in materials and colloid science, sensors, (photo)catalysis, electronics and medicine.[33-35] However, there are important challenges that remain unanswered in the application of POMs in medicine.[36] The most important is the thermodynamic and kinetic instability of POMs in aqueous environments at physiological pH.[37] Controlling the pH of the working solution is important for the formation of the POM framework, and there is a defined pH range in which the POMs remain stable. When POMs are exposed to neutral or basic pHs (such as physiological pH 7.4), they become unstable and degrade,[38, 39] and consequently lose their distinctive properties. Despite these drawbacks, recent work by Pei and coworkers[40-43] and other groups[44, 45] have indicated that some Gd-POMs have both attractive imaging properties and desirable pharmacokinetic behaviour. For example, $[Gd(W_5O_{18})_2]^{9-}$ (abbreviated as GdWO) has recently been utilised for MRI. GdWO has a reported r_1 value of 4.6 $s^{-1}mM^{-1}$ at 1.5T,[46] and 6.89 $s^{-1}mM^{-1}$ at 9.39T,[40] which is higher than clinically used Gd-DTPA (r_1 value of 3.3 $s^{-1}mM^{-1}$ at 1.5T).[47] Pei and coworkers data also suggests that, of the Gd-POMs examined, GdWO is stable over a broad a broader pH range, making it attractive as a clinically applied MRI contrast agent.[48, 49] However, GdWO was also found to have a lower LD_{50} than Gd-DTPA,[10], which the authors attributed to high anionic charge and instability of GdWO in solution.

To improve their toxicity profile and imaging properties, the incorporation of Gd-POMs into both biological and synthetic nanostructures has been proposed. For example, Lixin Wu and coworkers formed dendritic assemblies with an amphiphilic molecule (alkyl chain and PEG chain with a quaternary ammonium head group) and $K_{13}[Gd(\beta_2\text{-}SiW_{11}O_{39})_2]$. These researchers determined that the assemblies formed different structures depending on the polymer concentration, and displayed structure dependent relaxivities.[50-52] Chai *et al.* demonstrated that the r_1 of GdWO increased by a factor of 3 when encapsulated with a spermine based cationic homopolymer,[46] while Huang *et al.* introduced GdWO as the MRI contrast agent into a cationic polymer-DNA polyionic complex for transfection applications.[53] More recently, Yong *et al.* synthesised BSA@GdWO hybrid nanoparticles,[54] and GdWO conjugated chitosan hybrid nanoparticles,[55] and investigated them as a theranostic nanoprobe; demonstrating the utility of GdWO as both an imaging agent for MRI and CT, as well as a cancer therapeutic as a radio sensitiser. To the best of our knowledge, these are the only cases where Gd-POMs have been applied for enhancing MRI contrast to date.

It is important to note that while these works have examined the relaxivities of Gd-POMs, they have neglected to assess the effect of pH on the stability and relaxivity of the Gd-POMs studied. Indeed, these works did not provide the pH at which the relaxivity experiments were performed POMs are well-known to be unstable at physiological pH (7.4), it is crucial to develop strategies for stabilising POMs at physiological relevant pH so as to achieve optimum contrast and enable clinical use.

To address this, we report the analysis of GdWO at different pHs to investigate how pH affects the stability and imaging properties of GdWO. Further, we stabilised the GdWO by addition of a designed block copolymer comprising an antifouling 'stealth' brush mPEG block and a cationic, POMs binding block which leads to the formation of well-defined nano-assemblies. These nano-assemblies were characterised for their size, shape and surface chemistry and then a preliminary MRI investigation was undertaken to acquire the relaxivity and stability over time. Finally, the relaxivities of the selected nano-assemblies at different physiologically relevant pH were evaluated. These results revealed enhanced stability of the nano-assemblies at physiological pH, which is reflected by sustained high relaxivity across the pH range tested.

Experimental Section

Instrumentation

Attenuated total reflectance Fourier transform infrared spectroscopy (ATR-FTIR) spectra were recorded using Shimadzu IR Tracer-100 Fourier Transform Infrared spectrometer by averaging 512 scans at a resolution of 8 cm^{-1} in the MIR region of 4000-400 cm^{-1}.

X-ray photoelectron spectroscopy (XPS) was carried out on a Kratos AXIS Ultra photoelectron spectrometer with a monochromic Al Kα X-ray source (1486.6 eV) at 225 W (15 kv, 15 mA). The GdWO sample was ground to fine particles and mounted onto the grid. First a survey scan of the sample was conducted over a binding energy of 1200 – 0 eV with a pass energy of 160 eV at 1.0 eV steps and with 100 ms dwell time. Then the high resolution scans were taken at pass energy 20 eV, with 0.05 eV steps and dwell times of 500 – 2000 ms, depending on the species.

Thermogravimetric analysis (TGA) of the samples was performed on a Perkin-Elmer Thermogravimetric Analyzer (Pyris 1). Solid samples were heated from 25°C to 700°C at a constant temperature increase of 20°C/min using nitrogen as the furnace gas with a flow rate of 20 mL/min. The nano-assembly samples were prepared by dropping the nano-

assembly solution onto the TGA pans and drying the pans in an oven at 80°C. For the dialysed nano-assembly solution samples, dialysis was conducted with a 20 kDa Slide-A-Lyser MINI dialysis device against water over 2 days.

UV-Visible spectrophotometry (UV-Vis) was conducted on a Shimadzu UV-3600 UV-VIS-NIR spectrophotometer using quartz cuvettes with 10 mm path length.

Dynamic light scattering (DLS) measurements were carried out on a Malvern Zetasizer Nano ZS Series running DTS software (laser, 4 mW, λ = 633 nm; angle 173°). Samples were dispersed in water and measured at 25°C.

Transmission electron microscopy (TEM) images were recorded without staining using a Tecnai F20 or Tecnai F30 transmission electron microscope at an accelerating voltage of 200 kV at ambient temperature. A typical TEM grid preparation was conducted as follow: a 2 µL aliquot of a 0.1 wt% solution was dropped onto a Formvar-film copper grid (GSCu100F-50, Proscitech), after which samples were allowed to dry under air.

Magnetic resonance imaging (MRI) scans were taken using a 7T whole-body MRI scanner (MAGNETON 7T, Siemens Healthcare, Erlangen, Germany) using Nova single channel transmit with 32 receiver channels with an internal diameter of 18.5 cm and a 21 cm field of view along the z-direction. For the determination of the r_1, inversion recovery sequences were utilised with different inversion times (65, 200, 400, 500, 1000, 1500, 3000, and 4000 ms), TR = 5000 ms and TE 2.78 ms. All images were acquired with a 1 mm slice thickness, 150 × 112.5 mm FOV, 512 × 256 matrix size, and 1 average. Signal from each well was plotted as function of inversion time and fitted to a monoexponential inversion recovery curve to calculate T_1. The r_1 relaxivity for each material was calculated from the linear slope of a $1/T_1$ plotted as a function of calculation.

Inductively coupled plasma optical emission spectrometry (ICP-OES) was used to determine the amount of gadolinium ions in the materials using a Perkin-Elmer OPTIMA 7300 spectrometer. 50 µL of the sample was digested in 200 µL of nitric acid (70%) in a water bath at 70°C overnight. The samples were then diluted to give a final nitric acid concentration of 1.4%.

Proton nuclear magnetic resonance (^{1}H NMR) spectra were recorded on an Avance III Nanobay 400 Hz Bruker spectrometer coupled to a BACS automatic sample changer. Samples were dissolved in deuterated chloroform. Chemical shifts were measured in part per million and were referenced to an internal standard.

Gel permeation chromatography (GPC) was used to determine the molecular weight distribution of the polymers relative to polystyrene samples. Samples were dissolved in *N,N*-dimethylacetamide (DMAc, HPLC grade, 0.05% w/v 2,6-dibutyl-4-methylphenol 0.03% w/v LiBr) to a concentration of approximately 1 mg/mL and filtered through a 0.45 µm PTFE syringe filter. Analysis was performed on a Shimadzu modular system comprising a DGU-20A3R degasser unit, an SIL-20A HT autoinjector, a 50 × 7.8 mm 10 µm bead-size guard column followed by three 300 × 7.8 mm linear KF-805L columns (bead size: 10 µm, pore size maximum: 5000 Å pore size) and a RID-20A differential refractive-index detector using DMAc as the eluent (40 °C, flow rate=1 mL/min). Calibration was achieved with commercial narrow-polydispersity polystyrene standards ranging from 500 to 2 × 10^6 g mol^{-1}.

Materials

Sodium tungstate dihydrate ($Na_2WO_4{\cdot}2H_2O$, >99%), gadolinium chloride hexahydrate ($GdCl_3{\cdot}6H_2O$, 99%), acetic acid (>99.7%), 4-cyano-4-(phenylcarbonothioylthio)pentanoic acid (CPADB), poly(ethylene glycol) methyl ether methacrylate (OEGMA, M_n=500 g mol^{-1}), 2-(dimethylamino)ethyl methacrylate (DMAEMA, 98%) and toluene (anhydrous, 99.8%) were purchased from Sigma Aldrich (St. Louis, MO, USA) and used as received. 2,2-Azobis(2-methylpropionitrile) (AIBN, 98%) was recrystallised from methanol. Dialysis tubing Cellu-Sep T1/nominal MWCO:3500 was purchased from Cellu-Sep(Seguin, TX, USA). 50× Tris/Acetic Acid/EDTA (TAE) buffer and Certified™ Molecular Biology agarose was purchased from Bio-Rad (Hercules, CA, USA). 20 kDa Slide-A-Lyser MINI dialysis device was purchased from ThermoFisher Scientific (Waltham, MA, USA) All other solvents were purchased from Merck Millipore (Darmstadt, Germany) and were of analytic grade. Water was purified by a Millipore Milli-Q water purification system and had a resistivity of 18.2 MΩ·cm. MDA-MB231 cells was purchased from American Type Culture Collection (Manassas, VA, USA).

Synthesis of GdWO

Synthesis of GdWO was based on the published procedures of Yamase[56] and Peacock[57]. Briefly, sodium tungstate dihydrate (8.30 g, 2.51 × 10^{-2} mol) was dissolved in 20 mL of MilliQ water. The sodium tungstate solution was then adjusted to pH 7.4 using acetic acid, and then the beaker was covered with aluminum foil and then heated to 85°C. Gadolinium chloride hexahydrate (0.929 g, 2.51 × 10^{-3} mol) was dissolved in 2 mL of warm MilliQ water. A syringe pump was used to add the warm $GdCl_3$ solution (5 mL syringe, addition rate of 0.5 mL/hour) to the stirring and hot Na_2WO_4 solution. Once all added, the solution was taken off the heat and the final pH of the solution was 5.4. The solution was then cooled in an ice bath to form GdWO crystals. The GdWO was then dried down by gently blowing a stream of compressed air onto the solution. Finally, the GdWO was made in to a stock solution of 2.35 mg/mL.

Synthesis of cationic mPEG brush block copolymer by reversible addition fragmentation chain transfer (RAFT) polymerisation

Synthesis of mPEG brush macromolecular chain transfer (macroRAFT) agent with poly(ethylene glycol) methyl ether methacrylate (OEGMA). The polymerisation was carried out with the following stoichiometry: $[OEGMA]_0$ /$[CPADB]_0$/$[AIBN]_0$ = 28/1/0.1. OEGMA (16.00 g, 3.20 × 10^{-2} mol), CPADB (319 mg, 1.14 × 10^{-3} mol), AIBN (18.7 mg, 1.14 × 10^{-4} mol) and 102.5 mL of dry toluene was combined in a glass vial and was purged by sparging with N_2 for 90 mins. The solution was heated to 70°C for 24 hours. The polymer was purified by 5 precipitation/centrifugation cycles into large excess of 3:2 (v:v) mixture of diethyl ether and petroleum benzene (b.p. 40-60°C). The polymer was then placed in a vacuum oven overnight to remove residual solvent.

Synthesis of (POEGMA-b-PDMAEMA) by chain extension of macroRAFT agent with DMAEMA. Polymerisation was carried out with the following stoichiometry: $[DMAEMA]_0$ /$[macroRAFT]_0$/$[AIBN]_0$ = 115/1/0.1. DMAEMA (4.00 g, 2.55 × 10^{-2} mol), macroRAFT (2.48 g, 2.21 × 10^{-4} mol), AIBN (3.6 mg, 2.21 × 10^{-5} mol) and 13.1 mL of dry toluene was combined in a glass vial and purged by sparging with N_2 for 60 mins. The polymerisation solution was then divided into three glass vials, which were fastened with a rubber septa and wire, with the approximate volumes of 5 mL, 5 mL and 10 mL. To understand the kinetics of the polymerisation, the first vial containing 5 mL of polymerisation solution was heated to 70°C for a total of 10 hours with samples of the polymerisation solution taken at 0, 2, 4, 6, 8 and 10 hours. The second vial containing 5 mL and the third vial containing 10 mL were heated to 70°C for 90 mins and 4 hours, respectively. The polymers were purified by dialysis against acetone over 2 days, and then placed in a vacuum oven overnight to remove residual solvent.

Synthesis of the nano-assemblies

2 mL of polymer aqueous solution (100 mg/mL) was prepared and adjusted to pH 6.0 with HCl. Polymer solution was then added dropwise to 5 mL of GdWO aqueous solution (1 mg/mL) to give a final pH of approximately 6. Different amounts of polymer were added based on the charge ratio equation as established by Zhang *et al.*.[58] The assemblies had charge ratios of 0.2, 0.3, 0.4, 0.5, 0.7 and 0.9.

pH titration of GdWO

pH titration of the material was conducted to determine the most stable pH range for GdWO. Benchtop pH measurements were performed using a Mettler-Toledo SevenCompact pH/Ion S220 meter equipped with an InLab Semi-Micro pH electrode. 2 mL of GdWO aqueous solution was titrated against 0.1 M HCl or 0.1 M NaOH.

Preparation of MRI samples

MRI scans were taken from an aqueous dilution series prepared in a Costar 96-well assay block (3959, 1 mL well volume, round bottom). To limit artefacts, the backside of the assay block was filled with 3% agarose using the following procedure: 300 mL TAE buffer ×1 (40 mM tris base, 40 mM acetic acid, and 1 mM EDTA) was stirred and 9.0 g agarose was added into the solution. The agarose dispersion was heated in a microwave until the solution boiled. The solution was decanted into the backside of the 96-well assay block. The agarose solution was left to cool down in the assay block, until an agarose gel formed. Dilution series of GdWOs and Gd-DTPA were prepared in aqueous solution (5 dilutions, dilution factor 2, 0.75 mL each, highest concentration ~0.2 mM Gd^{3+}). The exact concentration of gadolinium in each dilution series was determined by ICP-OES.

Cytotoxicity studies

MDA-MB231 (breast cancer cell line) was cultured in 96-well culture plates with RPMI (Roswell Park Memorial Institute) 1640 Medium containing FBS (fetal bovine serum) at 37°C under humidified 5% CO_2 atmosphere. Cell viability was assessed using the AlamarBlue assay. Cells were seeded at a density of 5000 cells per well and incubated for 24 hours for cell attachment. The cells were washed twice with PBS (phosphate buffer saline) and incubated with different concentration of Gd^{3+} of the material for a further 24 hours at 37°C under 5% CO_2 atmosphere. The wells were then washed twice with PBS and replenished with cell culture medium containing 10 µL of AlamarBlue, and incubated for another 4 hours. The fluorescence was detected by exciting at 540-570 nm and the emission read at 580-610 nm using a microplate reader. The experiments were conducted in triplicate, and viability was calculated as the percent fluorescence relative to the untreated control cells.

Results and Discussion

Synthesis of GdWO

$[Gd(W_5O_{18})_2]^{9-}$ was synthesised based on methods previously described by Yamase *et al.*[56] and Peacock *et al.*,[57] however the addition of the warm gadolinium chloride solution to the heated sodium tungstate solution was achieved using a syringe pump to provide increased control of the rate of addition. After purification of GdWO, the GdWO crystals were redispersed into MilliQ water to give a final concentration of 2.35 mg/mL for handling. The synthesis of GdWO was confirmed using ATR-FTIR and XPS spectroscopy. Figure 1a shows the infrared spectra of GdWO, which was in agreement with previously published reports,[59] with the identification of a single W=O peak at wavenumber 936 cm^{-1}, and a band of W-O-W vibrational peaks in the wavenumber region 706 - 833 cm^{-1}. Figure S1 shows the XPS high resolution scans which are also in agreement with literature, with the identification of the Gd 4d and W 4f and a ratio of Gd:W atoms of 1:10 as expected. GdWO was examined by thermogravimetric analysis (TGA) generating a TGA curve as seen in Figure S2. The TGA curve generated is consistent with published works on metal oxide nanoparticles (such as iron oxide nanoparticles); with a rapid weight loss of 5.5% at 140°C corresponding to the free water molecules and weight loss of 4% between 140°C – 200°C corresponding to the bound water molecules.

Importantly, POMs are known to be unstable at physiological pH in aqueous systems. To investigate this, GdWO was titrated against dilute sodium hydroxide (NaOH) and dilute hydrochloric acid (HCl) to obtain a titration curve, which to the best of our knowledge, has not been previously published for this particular POM. The titration curve is shown in Figure 1b, where GdWO in aqueous solution has a pH of ca. 6 and is titrated against HCl or NaOH. Generally, titration curves of POMs have two distinctive end-points, which were detected at pH 5.4 and pH 10.4 for GdWO. The first end-point observed at pH 5.4 corresponds to the complete neutralisation of the acid protons ($H_9[Gd(W_5O_{18})_2]$ → $[Gd(W_5O_{18})_2]^{9-}$) and the second end point at pH 10.4 signifies the complete degradation of the polyanion ($[Gd(W_5O_{18})_2]^{9-}$ → WO_4^{2-}). Also, intermediate to the two main end-points, another end point was also observed at pH 6.5 This end-point is most

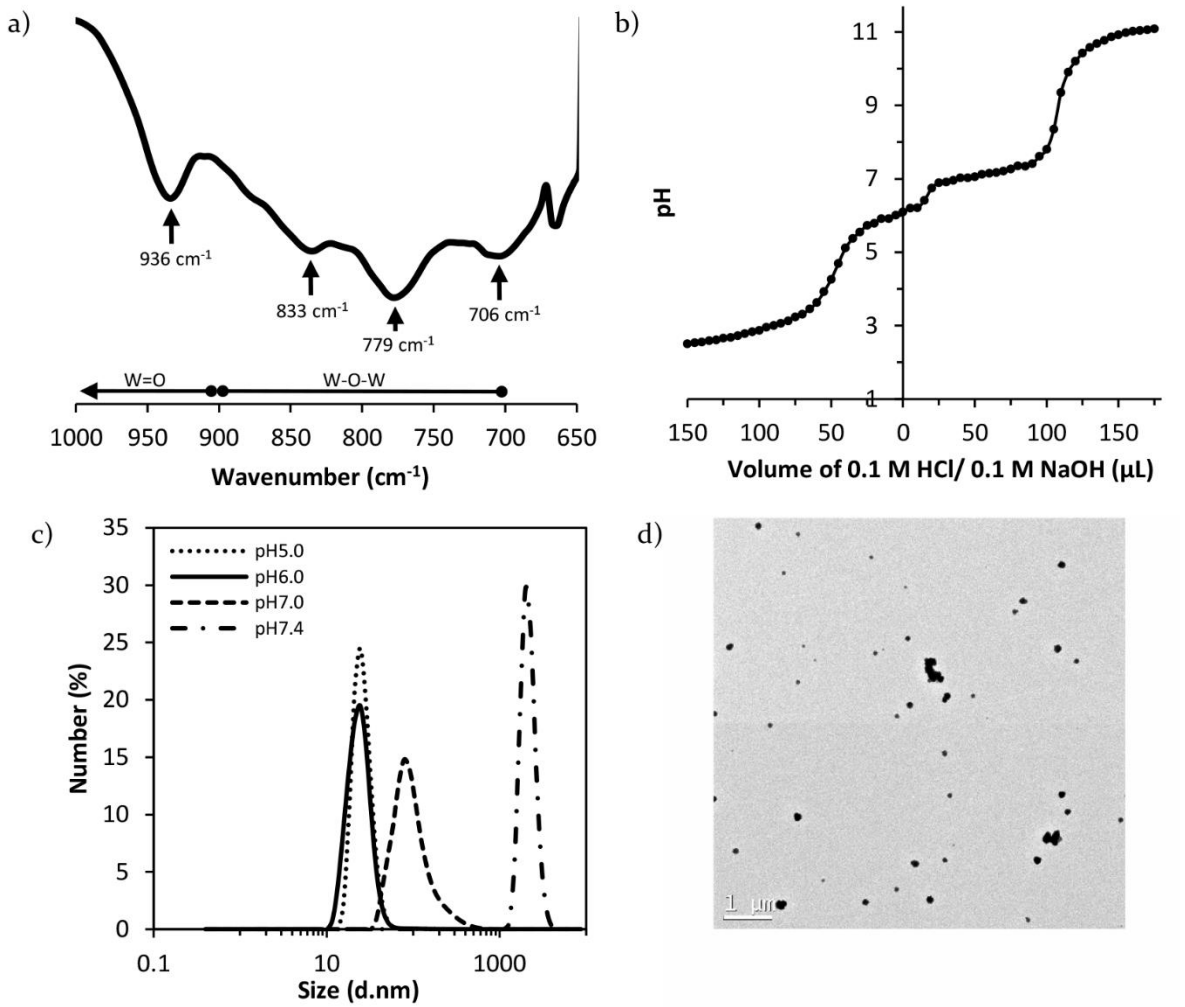

Figure 1 Characterisation of GdWO: ATR-FTIR spectra (a), titration curve (b), hydrodynamic size distribution at different pH (c) and TEM image (d).

likely attributed to the degradation of the GdWO sandwich framework to its subunit,[60] a Lindqvist monovacant derivative ($[Gd(W_5O_{18})_2]^{9-} \rightarrow GdW_5O_{18}^{3-} + W_5O_{18}^{6-}$). The UV-Vis spectra of GdWO at different pH also provides further evidence of the breakdown of the sandwich structure (Figure S3). The peak at 260 nm is monitored on the UV-Vis spectrophotometer as the pH of the GdWO solution is increased. There was no change of the intensity of the peak when the GdWO solution is adjusted from pH 5.9 to pH 6.3, but when the pH was increased to 6.4, the intensity of the peak at 260 nm begins to drop. The peak intensity continues to decrease until pH 6.6, after which there is no change in the peak intensity even up to pH 9.0. The change in the peak intensity at pH 6.4 indicates a transformation of the GdWO structure, and this also coincides with the titration end point involving the degradation of the sandwich structure. Correlation of the pH titration and UV-Vis spectroscopy data indicates that GdWO has a narrow pH range of optimal stability (pH 5.4-6.4), outside of which the GdWO can degrade to its building units (at high pH) or possibly form condensed clusters (at low pH).

Subsequently, GdWO solutions at different pHs were characterised by dynamic light scattering (DLS) and transmission electron microscopy (TEM) to elucidate the particle size and shape. The DLS number average size distribution (Figure 1c) indicates that GdWO has a hydrodynamic diameter of 25.7 nm at pH 6, which is suggestive of GdWO aggregation. This is supported by the TEM images showing large groups of small clusters with sizes varying from 70-170 nm (Figure 1d). Moreover, the hydrodynamic diameter of GdWO increased to 105.5 nm when the pH was increased to 7.0, until eventually only large aggregates above 1000 nm are observed at pH 7.4. The change in hydrodynamic diameter is attributed to the degradation of GdWO at basic pH, however, it is interesting to observe that the hydrodynamic diameter does not change at pH 5 (26.5 nm).

Next, the longitudinal relaxivity (r_1) of GdWO at pH 7.4, 6.0 and 5.0 was determined using a clinical 7T MRI scanner and ICP-OES to generate a relaxivity curve shown in Figure 2. At pH 6.0, GdWO has a r_1 of 8.86 $s^{-1}mM^{-1}$, which is 2 times higher than the clinical contrast agent Gd-DTPA, which has a r_1 of 4.43 $s^{-1}mM^{-1}$ when measured on the 7T system used here. The relaxivity of Gd-DTPA is known to be pH independent at pH>3, therefore the relaxivity of Gd-DTPA was not tested at different pH.[61] For GdWO, the solution was adjusted to pH 5.0, which yielded a

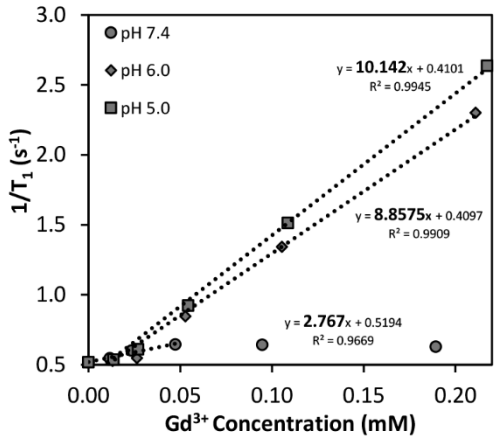

Figure 2 Relaxivity measurement of GdWO at pH 5.0, 6.0 and 7.4 on a 7T MRI scanner.

slight increase of the r_1 from 8.86 to 10.14 $s^{-1}mM^{-1}$. However, when GdWO was adjusted to pH 7.4, the relaxivity was reduced significantly to 2.77 $s^{-1}mM^{-1}$, likely due to the breakdown of the sandwich structure of GdWO, and the concomitant loss of imaging capabilities. Only the first three gadolinium concentrations (0.125, 0.25, 0.50 mM) were used to calculate the r_1 of GdWO at pH=7.4 due to the observed precipitation of GdWO at higher (0.6409 s^{-1} at 0.1 mM and 0.6285 s^{-1} at 0.2 mM). The demonstrated instability of GdWO and subsequent loss of contrasting ability highlights a significant drawback of GdWO if it is to be applied in biomedical imaging at physiological pH. Moreover, in certain tissues pH may even be as high as 8.[62, 63] Consequently, neat GdWO is unlikely to be an effective T_1 contrast agent despite displaying promising high relaxivity values at pH 6.0. To be suitable for biomedical imaging, GdWO needs to be stabilised to protect its structure as well as maintain its contrasting properties at physiological pH. As such, we explored the stabilisation of GdWO by employing a co-assembly/coating strategy with a designed cationic mPEG brush block copolymer.

Synthesis of the nano-assemblies

GdWO is a polyanion, with 9 negative charges, and as such we elected to prepare cationic block polymer to enable electrostatic binding to GdWO. DMAEMA, a tertiary amine-containing monomer with a pK_a = 8.44, was chosen due to the almost complete protonation of the tertiary amines at pH 6. However, homopolymers of DMAEMA are slightly cytotoxic due to its cationic nature, and for that reason, a PEG brush block was incorporated into the polymer design.[64] Furthermore, literature has also shown that PEGylation of nanoparticles can improve their biodistribution (through mechanisms such as decreasing uptake by the reticuloendothelial system, decreasing degradation via metabolic enzymes, and prolonging blood circulation etc.), leading to the enhancement of the therapeutic effect and/or imaging quality.[65-67] To this end, RAFT polymerisation was employed to synthesise a starting PEG brush block, followed by chain extension with DMAEMA to form the PDMAEMA domain (Scheme 1).

First, the mPEG brush macromolecular chain transfer ("macroRAFT") agent was synthesised with 22 OEGMA units, as determined by ^{1}H NMR. The macroRAFT agent was then chain extended with DMAEMA resulting in the POEGMA-b-PDMAEMA stabilising agents. Different lengths of the PDMAEMA domain were achieved by varying the polymerisation time: 1.5 hrs was used to provide 21 units of DMAEMA (denoted as $PDMAEMA_{20}$) while a polymerisation time of 4 hrs was used for 46 units of DMAEMA (denoted as $PDMAEMA_{40}$). The polymers were characterised by GPC to determine the molecular weight distribution and polydispersity, and ^{1}H NMR to confirm the composition (Table 1 and Figure S4).

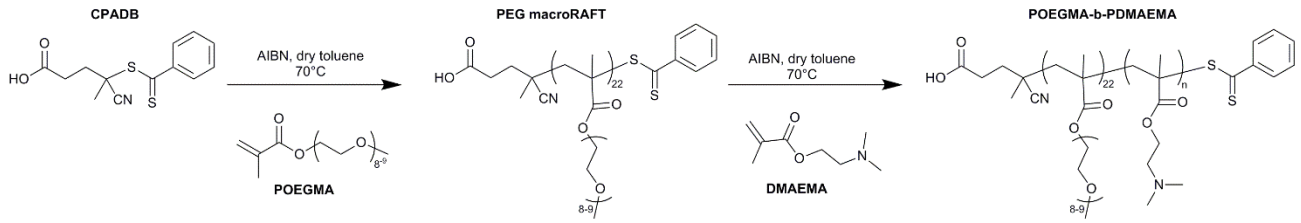

Scheme 1 RAFT polymerisation of the cationic mPEG brush block copolymer – POEGMA-b-PDMAEMA.

Table 1 Characterisation of RAFT polymers

Polymer	$[M]_0/[CTA]_0$ [a]	% monomer conversion [b]	M_n (theory) (Da) [c]	M_n (NMR) (Da) [d]	M_n (GPC) (Da) [e]	M_w/M_n [f]
POEGMA	28	68.6	9880	11200	11700	1.10
$POEGMA\text{-}b\text{-}PDMAEMA_{20}$	136	18.5	15150	14500	12300	1.11
$POEGMA\text{-}b\text{-}PDMAEMA_{40}$	136	34.6	18600	18400	14400	1.12

[a] Polymerisation [total monomers]=$[M]_0$; [RAFT agent]=$[CTA]_0$. [b] % Monomer conversion determined using ^{1}H NMR spectroscopy. [c] Theoretical number-average molecular weight: $M_n(theory) = ([M]_0/[CTA]_0) \times conversion \times (MW_{monomer}) + (MW_{RAFT\ agent})$. [d] ^{1}H NMR determined molecular weight by integration of 2 protons on the benzyl group (RAFT agent) and the protons of the monomers ($i_{4.1}$, $i_{3.4}$). The following equation was used for POEGMA $M_n(NMR) = (i_{4.1}/i_{7.9}) \times 500$. The following equation was used for POEGMA-b-PDMAEMA $M_n(NMR) = 11200 + 157.21[(3i_{4.1} - 2i_{3.4})/3i_{7.9}]$. [e] Determined by GPC analysis in DMAc using polystyrene standards. [f] Dispersity determined by GPC analysis in DMAc.

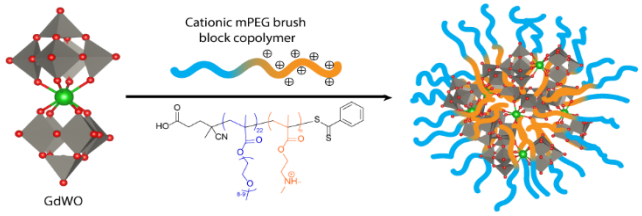

Scheme 2 Schematic illustration representing GdWO interacting with cationic mPEG brush block copolymer to form the nano-assemblies.

After synthesis, extensive purification by dialysis in acetone and full characterisation, the polymers were made up into aqueous solution at 100 mg/mL and adjusted to pH 6 with hydrochloric acid to provide the protonated form of the tertiary amine moieties (Scheme 2). The protonation of the tertiary amine also prevented the self-assembly of the polymers in aqueous solution, which was confirmed on the DLS (Figure S5). The polymer solution was then added dropwise to the stirring solution of GdWO, affording the nano-assemblies. Different amount of polymer were added to the solution based on Zhang *et al.*'s charge ratio equation: $\gamma = \frac{C_+}{C_+ + C_-}$ where C_+ is the moles of positive charge, and C_- is the moles of negative charge.[58] Six charge ratios were chosen for assembly of the polymers with GdWO: 0.2, 0.3, 0.4, 0.5, 0.7 and 0.9. The nano-assemblies are denoted as $^{[\text{charge ratio}]}P_{[\text{units of DMAEMA in polymer}]}$@GdWO; for example, the nano-assembly with $PDMAEMA_{20}$ and a charge ratio of 0.2 is denoted as $^{0.2}P_{20}$@GdWO. Theoretically, there are multiple GdWO nanocrystals per polymer chain for the nano-assemblies with charge ratio 0.2-0.5. While, $^{0.7}P_{20}$@GdWO and $^{0.9}P_{20}$@GdWO have 1 and 4 polymer chains per GdWO, respectively. $^{0.7}P_{40}$@GdWO and $^{0.9}P_{40}$@GdWO have 0.5 and 2 polymer chains per GdWO, respectively. TGA analysis of the nano-assemblies both before and after exhaustive purification by dialysis revealed the participation of all polymer chains in the formation of the nano-assemblies. Specifically, as seen in Figure S6, there is no difference in the TGA profiles of $^{0.2}P_{20}$@GdWO pre- and post-dialysis to remove free polymer chains.

DLS provided further evidence of the cationic polymer interacting with the GdWO, and forming assemblies as shown in Figure 3a for $PDMAEMA_{20}$ and Figure S7a for $PDMAEMA_{40}$. GdWO initially has a hydrodynamic diameter of ca. 26 nm, but when either $PDMAEMA_{20}$ or $PDMAEMA_{40}$ is introduced to the GdWO solution, the hydrodynamic diameter decreases to between 11-13.5 nm. This suggests that the polymer disrupts the aggregation and stabilises the GdWO. However at higher polymer/GdWO ratio of $^{0.9}P_{20}$@GdWO and $^{0.9}P_{40}$@GdWO, the formation of larger more complex assemblies was observed. TEM images of the $^{0.2}P_{20}$@GdWO nano-assemblies suggest the formation of spherical assemblies with sizes ranging from 4.7-22.4 nm (Figure 3b). TEM images of the other nano-assemblies can be seen in Figure S8. Figure 3c shows the ζ-potential of the P_{20}@GdWO nano-assemblies compared to the neat GdWO (-25.7 mV) and $PDMAEMA_{20}$ (+20.4 mV) revealing the expected charge inversion.

Preliminary investigation of the r_1 of the assemblies at pH 6 were conducted on a clinical 7T MRI machine to determine if the charge ratio and/or the length of the tertiary amine block polymer influences relaxivity. The r_1 of the P_{20}@GdWO and P_{40}@GdWO nano-assemblies were calculated and are given in Figure 4. All of the nano-assemblies have r_1 values higher than Gd-DTPA, however when compared to GdWO alone, only the nano-assemblies with charge ratio of 0.2 have a slightly higher r_1 (9.58 $s^{-1}mM^{-1}$ and 10.02 $s^{-1}mM^{-1}$ for $^{0.2}P_{20}$@GdWO and $^{0.2}P_{40}$@GdWO respectively). As the charge ratio of the nano-assemblies was increased to 0.3, 0.4 and 0.5, there is an observed decrease in the r_1. Above a charge ratio of 0.5, the r_1 of the nano-assemblies was found to increase. When comparing $PDMAEMA_{20}$ to $PDMAEMA_{40}$, there is no significant improvement of the r_1 between the nano-assemblies comprised of these two polymers. The P_{20}@GdWO series of nano-assemblies was therefore selected for further studies.

Stability of the nano-assemblies

The stability of the P_{20}@GdWO series of nano-assemblies was assessed by monitoring the hydrodynamic size on DLS and

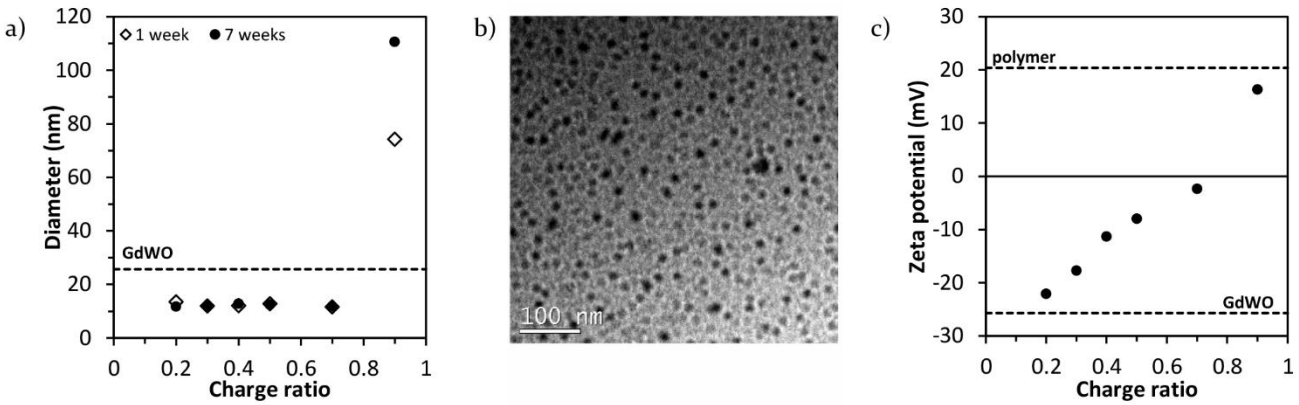

Figure 3 DLS determined number average particle size of P_{20}@GdWO nano-assemblies at week 1 and week 7 (a) followed by a TEM image of $^{0.2}P_{20}$@GdWO (b). DLS determined ζ-potential of the P_{20}@GdWO nano-assemblies (c).

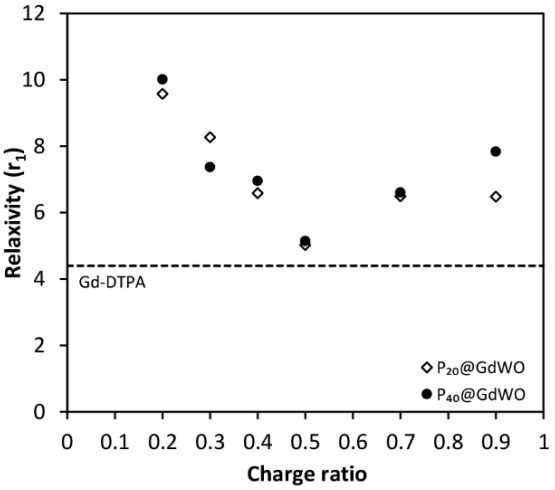

Figure 4 Relaxivity measurements of the P_{20}@GdWO and P_{40}@GdWO nano-assemblies at different charge ratios. The dotted line represents the r_1 of Gd-DTPA.

measuring the r_1 over the course of 7-10 weeks. Both techniques indicated that most of the P_{20}@GdWO nano-assemblies demonstrated stable aize and stability for at least 2 months. Figure 3a shows the hydrodynamic diameter of the assemblies at week 1, then at week 7. For the assemblies, except for $^{0.9}P_{20}$@GdWO, there is little change in the hydrodynamic diameter, with measurements in the range of 11.7-12.75 nm (corresponding to less than 12% change in size.) $^{0.9}P_{20}$@GdWO had a 49.0% increase in hydrodynamic size; from 74.24 to 110.6 nm indicating some instability at this higher charge ratio.

The P_{20}@GdWO nano-assembly dilution samples from the preliminary MRI study were stored at room temperature and in the dark after their initial MRI scan. The samples were rerun on the MRI machine ten weeks later, and the change in r_1 is given in Table 2. $^{0.2}P_{20}$@GdWO - $^{0.7}P_{20}$@GdWO showed little change in signal, with variation in relaxivity ranging from -3.5 to 2.3%. Once again, the exception is $^{0.9}P_{20}$@GdWO, as the r_1 decreased by 13.8% reflecting the fact that $^{0.9}P_{20}$@GdWO is unstable.

Table 2 Relaxivity measurement of the P_{20}@GdWO nano-assemblies at week 1 and 10

Nano-assembly	r_1 at pH 6 Week 1	r_1 at pH 6 Week 10	change in r_1
$^{0.2}P_{20}$@GdWO	9.36	9.58	2.3%
$^{0.3}P_{20}$@GdWO	8.20	8.28	1.0%
$^{0.4}P_{20}$@GdWO	6.56	6.59	0.4%
$^{0.5}P_{20}$@GdWO	4.98	5.03	0.9%
$^{0.7}P_{20}$@GdWO	6.73	6.49	-3.5%
$^{0.9}P_{20}$@GdWO	7.52	6.48	-13.8%

Relaxivity study of the nano-assemblies at different pH

The nano-assemblies were assessed at pH 7.4, 6.0 and 5.0 on the 7T MRI scanner to investigate the ability of the block copolymer to stabilise the GdWO, and maintain the r_1 signal at physiologically relevant pHs. As demonstrated earlier, GdWO loses its functionality as a contrast agent at physiological pH and as such is unsuitable for clinical application. In contrast, the P_{20}@GdWO nano-assemblies were found to be very stable in the pH range 5.0-7.4, with sustained high relaxivity as evident in Figure 5 and 6.

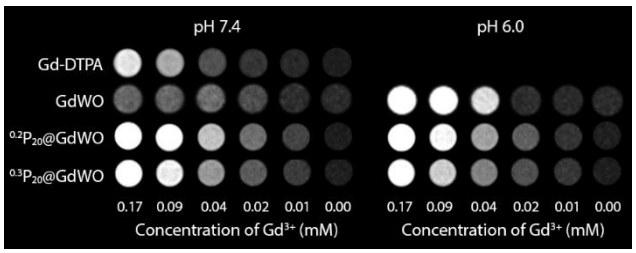

Figure 5 T_1-weighted MRI phantom images of Gd-DTPA, GdWO and the selected nano-assemblies $^{0.2}P_{20}$@GdWO and $^{0.3}P_{20}$@GdWO at pH 7.4 and pH 6.0. Gd-DTPA is not affected by pH, thus, there is only a phantom image at pH 7.4.

Figure 5 presents the MRI phantom image as a visual indicator of the effectiveness of the nano-assemblies as contrast agents. Generally for T_1-weighted images, the brighter the image at lower concentration, the more effective the contrast agent. When comparing the brightness of GdWO at pH 7.4 and pH 6.0, it is evident that GdWO loses it's contrasting properties significantly at pH 7.4. The MRI phantoms of the $^{0.2}P_{20}$@GdWO and $^{0.3}P_{20}$@GdWO are also compared; these were chosen as the preliminary MRI relaxivity data indicated that they had the highest r_1 value. At pH 7.4, the phantom images of $^{0.2}P_{20}$@GdWO and $^{0.3}P_{20}$@GdWO are much brighter than neat GdWO, suggesting that the polymer is not only protecting GdWO, but also maintaining its contrasting properties against changes in pH. The phantom images were then used to determine r_1 values for all the nano-assemblies and GdWO at different pHs, with the values given in Figure 6. GdWO itself performed better at pH 5.0 and pH 6.0 than most of the P_{20}@GdWO nano-assemblies, with the exception of $^{0.2}P_{20}$@GdWO. However, at pH 7.4, the P_{20}@GdWO nano-assemblies had an r_1 value 2-4 times higher than neat GdWO.

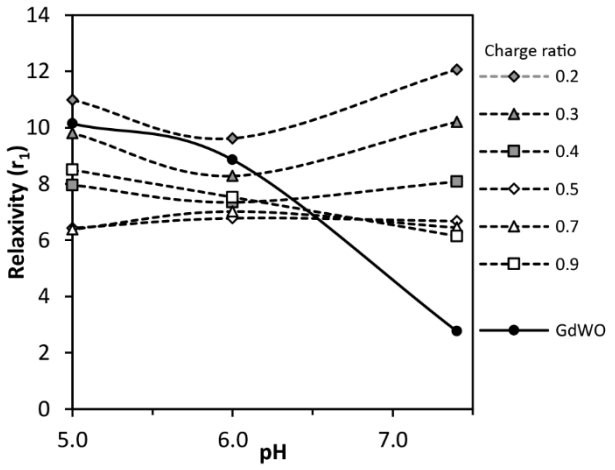

Figure 6 Relaxivity study of the P_{20}@GdWO nano-assemblies com-pared to GdWO at pH 5.0, 6.0 and 7.4. Line is not fitted data, only guidance for the eye.

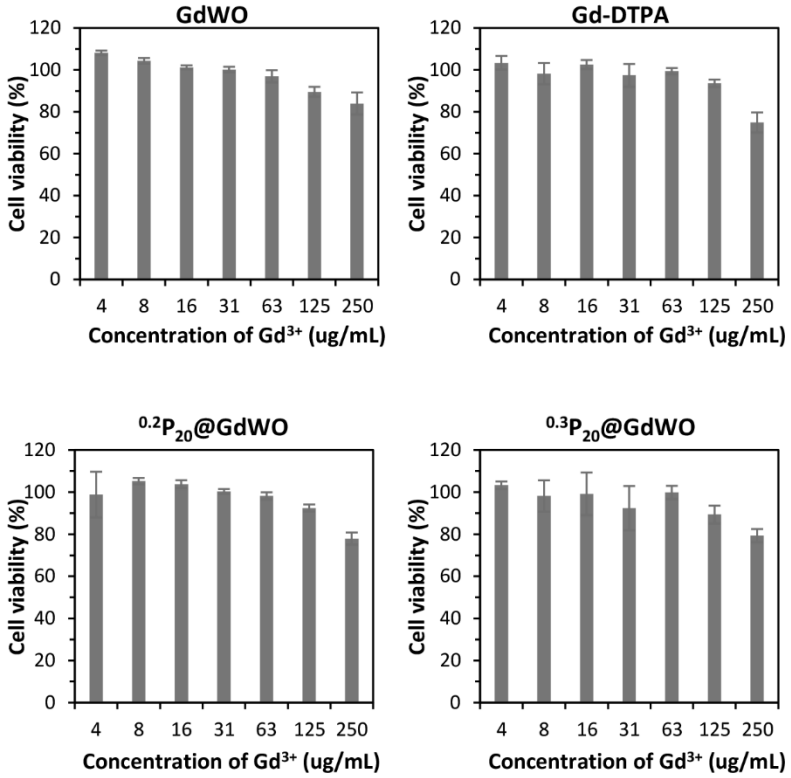

Figure 7 Cytotoxicity study of GdWO, Gd-DTPA and the nano-assemblies with AlamarBlue assay

Focusing at pH 7.4, the P_{20}@GdWO nano-assemblies show evidence of the charge ratio influencing the r_1. At low charge ratio (ie. multiple GdWO per chain), there is enhancement of the r_1 of the nano-assemblies, as observed for $^{0.2}P_{20}$@GdWO, $^{0.3}P_{20}$@GdWO and $^{0.4}P_{20}$@GdWO. Then, for $^{0.5}P_{20}$@GdWO, $^{0.7}P_{20}$@GdWO and $^{0.9}P_{20}$@GdWO, there is an inversion of the trend – r_1 decreases as the charge ratio increases. This suggests that the polymer concentration, which dictates the formation of the nano-assemblies, affects the relaxivity of the nano-assemblies. The formation of the nano-assemblies may influence the interaction of the embedded GdWO with the surrounding water molecules (one of the key mechanism for gadolinium ions as a contrast agents), resulting in either an enhancement or reduction of the r_1. Once again, $^{0.9}P_{20}$@GdWO is an exception demonstrating a linear relationship between r_1 and pH; a r_1 of 8.50 $s^{-1}mM^{-1}$ at pH 5.0, 7.53 $s^{-1}mM^{-1}$ at pH 6.0 and then 6.15 $s^{-1}mM^{-1}$ at pH 7.4. Altogether, most of the P_{20}@GdWO nano-assemblies are stable at physiologically relevant pH and have a higher r_1 value than Gd-DTPA across all pHs studies, in stark contrast to neat GdWO.

Cytotoxicity studies

Finally the cytotoxicity of GdWO, polymer and the nano-assemblies were evaluated using the AlamarBlue assay on MDA-MB231 (breast cancer cell line) cells. As shown in Figure 7, the cells tolerated the neat GdWO and Gd-DTPA with a slight decrease of the cell viability at the highest concentration investigated. The cells were treated with the P_{20}@GdWO nano-assemblies based on the concentration of the Gd^{3+}; with most nano-assemblies being well tolerated by the cells. The toxic nature of $^{0.9}P_{20}$@GdWO is likely due to the high cationic polymer content, and as such, $^{0.9}P_{20}$@GdWO is unlikely to be suitable as a nano-assembly for MRI imaging. The low charge ratio nano-assemblies, $^{0.2}P_{20}$@GdWO and $^{0.3}P_{20}$@GdWO, were most biocompatible showing cell viability just under 80% at the highest tested gadolinium concentration. As such, the observed biocompatibility of $^{0.2}P_{20}$@GdWO and $^{0.3}P_{20}$@GdWO suggests that they are potential candidates for application as contrast agents.

Conclusions

In conclusion, we have demonstrated that GdWO exhibits the properties of an effective contrast agent at pHs below 6.4. However, above this pH, the structure of GdWO becomes compromised, resulting in insufficient shortening of the longitudinal relaxation time and essentially rendering GdWO useless as a contrast agent. To ameliorate this deficiency, GdWO was assembled with mPEG brush block copolymer with a cationic segment at different charge ratios to prepare a series of hybrid GdWO nano-assemblies. We have demonstrated that the observed r_1 of the prepared nano-assemblies was charge ratio dependent, but that the length of the cationic polymer block does not affect r_1 within the range of block lengths tested. Representative P_{20}@GdWO nano-assemblies were examined for stability, relaxivity and cytotoxicity studies. With the exception of $^{0.9}P_{20}$@GdWO, the P_{20}@GdWO nano-assemblies showed good stability, with no major change in r_1 or size over 10 weeks and good r_1 at physiologically relevant pH. The best performing nano-assembly in terms of stability, high relaxivity

and low cytotoxicity was $^{0.2}P_{20}$@GdWO, making it a suitable and promising nano-assembly for further *in vivo* studies. This research demonstrates the important impact of pH on POMs for MRI applications, and the potential for using well-defined polymeric stabilisers to enable use of POMs at physiologically relevant pHs.

Conflicts of interest

There are no conflicts to declare.

Acknowledgements

Inductively coupled plasma optical emission spectrometry was performed at the Mark Wainwright Analytical Centre, University of New South Wales by Ms. Rabeya Akter. Electron microscopy was performed at the Bio21 Advanced Microscopy Facility, The University of Melbourne by Dr. Nghia Truong and Mr. Song Yang Khor. J.L. would like to thank Dr. Lars Esser for their guidance for designing and analysing the MRI experiments. This work was carried out within the Australian Research Council (ARC) Centre of Excellence in Convergent Bio-Nano Science and Technology (Project No. CE140100036). J.L. acknowledges the financial support from the Australian Government Research Training Program Scholarship. B.A.M is supported by a National Imaging Facility (NIF) Fellowship and the 7T MRI is part of The University of Melbourne node of NIF funded through the Australian Government NCRIS program. J.F.Q. acknowledges receipt of a Future Fellowship from the ARC (FT170100144). T.P.D. is grateful for the award of an Australian Laureate Fellowship from the ARC.

References

1. J. Cheon and J.-H. Lee, *Accounts of Chemical Research*, 2008, **41**, 1630-1640.
2. J. Key and J. F. Leary, *International Journal of Nanomedicine*, 2014, **9**, 711-726.
3. T. F. Massoud and S. S. Gambhir, *Genes & Development*, 2003, **17**, 545-580.
4. P. C. Lauterbur, *Nature*, 1973, **242**, 190-191.
5. P. A. Rinck, The Basic Textbook of the European Magnetic Resonance Forum, 8th edition edn., 2014.
6. OCED, *Magnetic resonance imaging (MRI) exams*, OCED Publishing 2017.
7. S. C. Bushong, *Magnetic Resonance Imaging: Physical and Biological Principles*, Mosby2003.
8. D. W. McRobbie, E. A. Moore, M. J. Graves and M. R. Prince, *MRI from Picture to Proton*, Cambridge University Press2007.
9. P. Caravan, J. J. Ellison, T. J. McMurry and R. B. Lauffer, *Chem. Rev.*, 1999, **99**, 2293-2352.
10. H. J. Weinmann, R. C. Brasch, W. R. Press and G. E. Wesbey, *American Journal of Roentgenology*, 1984, **142**, 619-624.
11. P. Marckmann, L. Skov, K. Rossen, A. Dupont, M. B. Damholt, J. G. Heaf and H. S. Thomsen, *Journal of the American Society of Nephrology*, 2006, **17**, 2359-2362.
12. F. Carniato, L. Tei, M. Cossi, L. Marchese and M. Botta, *Chemistry-a European Journal*, 2010, **16**, 10727-10734.
13. A. Mignot, C. Truillet, F. Lux, L. Sancey, C. Louis, F. Denat, F. Boschetti, L. Bocher, A. Gloter, O. Stephan, R. Antoine, P. Dugourd, D. Luneau, G. Novitchi, L. C. Figueiredo, P. C. de Morais, L. Bonneviot, B. Albela, F. Ribot, L. Van Lokeren, I. Dechamps-Olivier, F. Chuburu, G. Lemercier, C. Villiers, P. N. Marche, G. Le Duc, S. Roux, O. Tillement and P. Perriat, *Chemistry-a European Journal*, 2013, **19**, 6122-6136.
14. C. Alric, J. Taleb, G. L. Duc, C. Mandon, C. Billotey, A. L. Meur-Herland, T. Brochard, F. Vocanson, M. Janier, P. Perriat, S. Roux and O. Tillement, *Journal of the American Chemical Society*, 2008, **130**, 5908-5915.
15. M. Beija, Y. Li, H. T. Duong, S. Laurent, L. V. Elst, R. N. Muller, A. B. Lowe, T. P. Davis and C. Boyer, *Journal of Materials Chemistry*, 2012, **22**, 21382-21386.
16. M. Tsotsalas, M. Busby, E. Gianolio, S. Aime and L. De Cola, *Chemistry of Materials*, 2008, **20**, 5888-5893.
17. P. J. Endres, T. Paunesku, S. Vogt, T. J. Meade and G. E. Woloschak, *Journal of the American Chemical Society*, 2007, **129**, 15760-15761.
18. G. Ratzinger, P. Agrawal, W. Koerner, J. Lonkai, H. M. H. F. Sanders, E. Terreno, M. Wirth, G. J. Strijkers, K. Nicolay and F. Gabor, *Biomaterials*, 2010, **31**, 8716-8723.
19. L. Esser, N. P. Truong, B. Karagoz, B. A. Moffat, C. Boyer, J. F. Quinn, M. R. Whittaker and T. P. Davis, *Polymer Chemistry*, 2016, **7**, 7325-7337.
20. Y. Li, S. Laurent, L. Esser, L. V. Elst, R. N. Muller, A. B. Lowe, C. Boyer and T. P. Davis, *Polymer Chemistry*, 2014, **5**, 2592-2601.
21. Y. Li, M. Beija, S. Laurent, L. vander Elst, R. N. Muller, H. T. T. Duong, A. B. Lowe, T. P. Davis and C. Boyer, *Macromolecules*, 2012, **45**, 4196-4204.
22. Y. Li, H. T. T. Duong, S. Laurent, A. MacMillan, R. M. Whan, L. V. Elst, R. N. Muller, J. Hu, A. Lowe, C. Boyer and T. P. Davis, *Advanced Healthcare Materials*, 2015, **4,** 148-156.
23. J. Y. Park, M. J. Baek, E. S. Choi, S. Woo, J. H. Kim, T. J. Kim, J. C. Jung, K. S. Chae, Y. Chang and G. H. Lee, *Acs Nano*, 2009, **3**, 3663-3669.
24. P. Vahdatkhah, H. R. M. Hosseini, A. Khodaei, A. R. Montazerabadi, R. Irajirad, M. A. Oghabian and H. H. Delavari, *Chemical Physics*, 2015, **453**, 35-41.
25. H. Hifumi, S. Yamaoka, A. Tanimoto, T. Akatsu, Y. Shindo, A. Honda, D. Citterio, K. Oka, S. Kuribayashi and K. Suzuki, *Journal of Materials Chemistry*, 2009, **19**, 6393-6399.
26. Y. I. Park, J. H. Kim, K. T. Lee, K.-S. Jeon, H. Bin Na, J. H. Yu, H. M. Kim, N. Lee, S. H. Choi, S.-I. Baik, H. Kim, S. P. Park, B.-J. Park, Y. W. Kim, S. H. Lee, S.-Y. Yoon, I. C. Song, W. K. Moon, Y. D. Suh and T. Hyeon, *Advanced Materials*, 2009, **21**, 4467-4471.
27. J. Ryu, H.-Y. Park, K. Kim, H. Kim, J. H. Yoo, M. Kang, K. Im, R. Grailhe and R. Song, *Journal of Physical Chemistry C*, 2010, **114**, 21077-21082.
28. S. G. Boyes, M. D. Rowe, C.-C. Chang, D. H. Thamm, S. L. Kraft, J. F. Harmon, Jr., N. J. Serkova, A. P. Vogt and B. S. Sumerlin, in *Polymeric Delivery of Therapeutics*, eds. S. E. Morgan and R. Y. Lochhead2010, vol. 1053, pp. 65-101.
29. W. Hatakeyama, T. J. Sanchez, M. D. Rowe, N. J. Serkova, M. W. Liberatore and S. G. Boyes, *Acs Applied Materials & Interfaces*, 2011, **3**, 1502-1510.

30. M. D. Rowe, C.-C. Chang, D. H. Thamm, S. L. Kraft, J. F. Harmon, Jr., A. P. Vogt, B. S. Sumerlin and S. G. Boyes, *Langmuir*, 2009, **25**, 9487-9499.
31. L. Zhu, Y. Yang, K. Farquhar, J. Wang, C. Tian, J. Ranville and S. G. Boyes, *Acs Applied Materials & Interfaces*, 2016, **8**, 5040-5050.
32. J. J. Berzelius, *Annalen der Physik*, 1826, **82**, 369-392.
33. J. J. Borrás-Almenar, *Polyoxometalate Molecular Science*, Dordrecht : Springer Netherlands : Imprint : Springer, Dordrecht, 2003.
34. D. L. Long, R. Tsunashima and L. Cronin, *Angewandte Chemie-International Edition*, 2010, **49**, 1736-1758.
35. M. T. Pope and A. Muller, *Angewandte Chemie-International Edition in English*, 1991, **30**, 34-48.
36. C. L. Hill, *Chem. Rev.*, 1998, **98**, 1-2.
37. J. T. Rhule, C. L. Hill, D. A. Judd and R. F. Schinazi, *Chem. Rev.*, 1998, **98**, 327-358.
38. L. C. W. Baker and D. C. Glick, *Chem. Rev.*, 1998, **98**, 3-50.
39. G. Hervé, A. Tézé and R. Contant, in *Polyoxometalate Molecular Science*, eds. J. J. Borrás-Almenar, E. Coronado, A. Müller and M. Pope, Springer Netherlands, Dordrecht2003, pp. 33-54.
40. J. Feng, X. Li, F. Pei, G. Sun, X. Zhang and M. Liu, *Magn. Reson. Imaging*, 2002, **20**, 407-412.
41. J. Feng, G. Sun, F. Pei and M. Liu, *J. Inorg. Biochem.*, 2002, **92**, 193-199.
42. Z. Li, W. Li, X. Li, F. Pei, Y. Li and H. Lei, *Magn. Reson. Imaging*, 2007, **25**, 412-417.
43. G. Sun, J. Feng, H. Wu, F. Pei, K. Fang and H. Lei, *Magn. Reson. Imaging*, 2004, **22**, 421-426.
44. K. Da-liang, W. Bo, Z. Sheng-yan, Y. Hai-shan and J. Yang, *Chem. Res. Chin. Univ.*, 2013, **29**, 1055-1058.
45. W. J. Crooks, G. R. Choppin, B. E. Rogers and M. J. Welch, *Nuclear Medicine and Biology*, 1997, **24**, 123-125.
46. W. Chai, S. Wang, H. Zhao, G. Liu, K. Fischer, H. Li, L. Wu and M. Schmidt, *Chem. - Eur. J.*, 2013, **19**, 13317-13321.
47. M. Rohrer, H. Bauer, J. Mintorovitch, M. Requardt and H. J. Weinmann, *Investigative Radiology*, 2005, **40**, 715-724.
48. J. H. Feng, X. J. Li, F. Y. Jing and F. K. Pei, *Acta Chim. Sin.*, 2000, **58**, 423-426.
49. Z. Li, X. Li, W. Li, P. Liao, L. Wei, J. FY. and F. Pei, *Journal of Molecular Science*, 2002, **22**, 76-79.
50. Y. L. Wang, S. Y. Zhou, D. L. Kong, H. S. Yang, W. Q. Chai, U. Kortz and L. X. Wu, *Dalton Transactions*, 2012, **41**, 10052-10059.
51. S. Zhang, Y. Zheng, D.-Y. Fu, W. Li, Y. Wu, B. Li and L. Wu, *Journal of Materials Chemistry B*, 2017, **5**, 4035-4043.
52. S. M. Zhang, Y. M. Zheng, S. Y. Yin, J. Z. Sun, B. Li and L. X. Wu, *Chemistry-a European Journal*, 2017, **23**, 2802-2810.
53. Y. J. Huang, H. Hu, R. Q. Li, B. R. Yu and F. J. Xu, *Acs Applied Materials & Interfaces*, 2016, **8**, 3919-3927.
54. Y. Yong, L. Zhou, S. Zhang, L. Yan, Z. Gu, G. Zhang and Y. Zhao, *NPG Asia Mater*, 2016, **8**, e273.
55. Y. Yong, C. Zhang, Z. Gu, J. Du, Z. Guo, X. Dong, J. Xie, G. Zhang, X. Liu and Y. Zhao, *ACS Nano*, 2017, **11**, 7164-7176.
56. T. Yamase and T. Ozeki, *Acta Crystallographica Section C-Crystal Structure Communications*, 1993, **49**, 1577-1580.
57. R. D. Peacock and T. J. R. Weakley, *Journal of the Chemical Society A: Inorganic, Physical, Theoretical*, 1971, 1836-1839.
58. J. Zhang, Y. Liu, Y. Li, H. Zhao and X. Wan, *Angewandte Chemie International Edition*, 2012, **51**, 4598-4602.
59. C. M. Granadeiro, R. A. S. Ferreira, P. C. R. Soares-Santos, L. D. Carlos, T. Trindade and H. I. S. Nogueira, *J. Mater. Chem.*, 2010, **20**, 3313-3318.
60. M. H. Alizadeh, H. Eshtiagh-Hosseini and R. Khoshnavazi, *Journal of Molecular Structure*, 2004, **688**, 33-39.
61. X. Zhang, C. A. Chang, H. G. Brittain, J. M. Garrison, J. Telser and M. F. Tweedle, *Inorganic Chemistry*, 1992, **31**, 5597-5600.
62. I. F. Tannock and D. Rotin, *Cancer Research*, 1989, **49**, 4373-4384.
63. T. Volk, E. Jahde, H. P. Fortmeyer, K. H. Glusenkamp and M. F. Rajewsky, *British Journal of Cancer*, 1993, **68**, 492-500.
64. J. M. Hu, G. Y. Zhang, Z. S. Ge and S. Y. Liu, *Progress in Polymer Science*, 2014, **39**, 1096-1143.
65. J. V. Jokerst, T. Lobovkina, R. N. Zare and S. S. Gambhir, *Nanomedicine*, 2011, **6**, 715-728.
66. A. S. Karakoti, S. Das, S. Thevuthasan and S. Seal, *Angewandte Chemie-International Edition*, 2011, **50**, 1980-1994.
67. A. Kolate, D. Baradia, S. Patil, I. Vhora, G. Kore and A. Misra, *Journal of Controlled Release*, 2014, **192**, 67-81.